


Article

Research on the Failure Mechanisms and Strength Characteristics of Deeply Buried Mudstone under the Interaction of Water and Stress

Yuedong Liu ^{1,2,*}  and Dongpan Wang ^{1,2}¹ CCTEG Coal Mining Research Institute, Beijing 100013, China² Mining and Design Department, Tiandi Science and Technology Company Ltd., Beijing 100013, China

* Correspondence: liuyuedong@tdkcsj.com

Abstract: Mudstone is a widely occurring type of rock in deep mining, and it is crucial to understand its failure mechanisms and strength characteristics under the interaction of water and high stress to ensure the stability of deeply buried engineered mudstone. In this study, the composition and the structure of mudstone were obtained, and triaxial tests were conducted on mudstone under five different water contents and four different confining pressures using a triaxial servo press. The variation rules for the peak strength and residual strength were obtained, and the applicability of the strength criteria was analyzed through fitting. The results showed that both the peak strength and the residual strength decreased linearly with increasing water content, with the peak strength decreasing more rapidly. Both the peak strength and the residual strength increased with increasing confining pressure, with the residual strength increasing more rapidly. The decrease in strength was primarily due to the decrease in cohesion, with the cohesion of the peak strength decreasing from 8.40 MPa to 0.94 MPa and the cohesion of the residual strength decreasing from 1.75 MPa to 0.82 MPa. The internal friction angle did not change much, with the internal friction angle of the peak strength decreasing from 41.57° to 37.29° and the internal friction angle of the post-peak strength increasing from 32.35° to 33.28°. For dry and low-water-content mudstone, the peak strength conformed to the Mohr–Coulomb criterion, while for mudstone with a higher water content, the peak strength conformed to the Hoek–Brown criterion. The residual strength conformed to the Hoek–Brown criterion. Under low and medium confining pressures, water played a dominant role in the damage pattern for the fractures produced by the initial damage to the mudstone. Under a high perimeter pressure, water played a guiding role for the fractures produced by the initial damage to the mudstone.

Keywords: mudstone; deep mining; failure mechanism; strength characteristic; water

Citation: Liu, Y.; Wang, D. Research on the Failure Mechanisms and Strength Characteristics of Deeply Buried Mudstone under the Interaction of Water and Stress.

Processes **2023**, *11*, 1231. <https://doi.org/10.3390/pr11041231>

Academic Editors: Andrea Spagnoli, Junwen Zhang, Xuejie Deng and Zhaohui Wang

Received: 8 March 2023

Revised: 30 March 2023

Accepted: 12 April 2023

Published: 16 April 2023



Copyright: © 2023 by the authors. Licensee MDPI, Basel, Switzerland. This article is an open access article distributed under the terms and conditions of the Creative Commons Attribution (CC BY) license (<https://creativecommons.org/licenses/by/4.0/>).

1. Introduction

Mudstone is a commonly used type of rock in deeply buried projects due to the various abundant clay minerals it possesses. However, its mechanical strength is low and deteriorates rapidly when exposed to water. Therefore, studying the failure mechanisms and strength characteristics of deeply buried mudstone under a hydraulic coupling action is crucial for ensuring its stability in deeply buried mudstone projects.

Currently, the linear Mohr–Coulomb (M–C) criterion [1] and the nonlinear Hoek–Brown (H–B) criterion [2,3] are the most widely used theories in theoretical analyses and in numerical simulation software for geotechnical engineering. The parameters, or variables, are fitted and reversed by a triaxial test of rock mechanics. Singh [4,5] conducted an investigation into the M–C criterion for intact rock and concluded that the criterion did not take into account the effect of intermediate principal stress. Subsequently, he proposed modifications to the M–C criterion to improve its applicability to rock mass. Building

on the H–B criterion for intact rock, Hoek [6,7] proposed engineering geological parameters (GSI) and blasting disturbance parameters (D) to extend the criterion to rock mass. Some scholars have extended this failure criterion by adding the influence of intermediate principal stress [8,9]. Six different data-driven machine learning models were established to predict and study the failure of intact rock materials under multi-axial (true triaxial) stress conditions [10]. Subsequent research [11,12] has explored the application conditions of this criterion, with the introduction of additional parameters or variables resulting in improved fitting; however, these parameters or variables are difficult to obtain and lack specific physical significance.

The residual strength of damaged mudstone has great influence on mudstone engineering. Sun Chuang [13] investigated the residual strength of damaged mudstone and its implications for mudstone engineering. He incorporated the post-peak nonlinear change characteristics of mudstone under varying dilatancy angles into the M–C strain-softening model. Wang Laigui [14] examined the effect of water content and confining pressure on the residual strength degradation coefficient of mudstone and derived an attenuation equation based on the correlation coefficients of various fitting functions. Cai and Walton [15,16] suggested that the H–B criterion may be better suited to describe the relationship between residual strength and confining pressure. Following rock failure, strength and cohesion decrease while the angle of internal friction exhibits two distinct changes: one is nearly unchanged [17,18] and the other is reduced [19]. Zhang Houquan [20] investigated the damage process through tests and elucidated the causes of these two changes. Xiong [21] investigated the rock parameters of mudstone, sandy mudstone, and sandstone in coal measure strata before and after water absorption and discovered that after water absorption, the cohesion decreased significantly while the internal friction angle changed only slightly. This was attributed to cohesion being the structural parameter and the friction coefficient being the material parameter. Scholars have studied the failure forms of mudstone. Zhu [22] studied the tensile fracture of water-bearing rocks through acoustic emissions. M.P. [23] compared the floor heave of a roadway under dry and water-bearing conditions and established a model. Wang [24] considered the dynamic characteristics and failure mechanism of coal under water static–dynamic coupling loads. Luo [25] conducted an experimental study on the stress failure of a hard rock roadway under water-bearing and true triaxial compression. Xue [26] considered the damage caused by pore pressure to a coal rock mass. It has been shown that the failure of mudstone is affected by multi-factor coupling, but the degree of water content has the greatest influence.

Previous studies have mainly focused on the peak strength and residual strength of rocks. In this paper, based on disintegrated mudstone, we investigate the change law of the peak strength and post-peak strength of mudstone under different water contents and confining pressures through experiments, select the fracture criterion, and determine the influence weight of the water content and confining pressure based on the failure form and degree.

2. Failure Mechanism and Strength Characteristics of Deeply Buried Mudstone under the Interaction of Water and Stress

The Sijiazhuang mine is located in Xiyang County, Yangquan City, Shanxi Province, and has a well field area of 124.08 km² and a high gas mine with an annual design capacity of 6 Mt/a. The samples selected in this study were taken from the 15,301 working faces of the Sijiazhuang mine, the roof of the roadway was 8 m away from the floor of the number 15 coal seam, the burial depth was approximately 623 m, and the design length was 2392 m. An anchor net cable support was adopted, and the roadway surrounding the rock was mainly mudstone, which is prone to disintegration upon contact with water, resulting in roadway pumping, as illustrated in Figure 1.

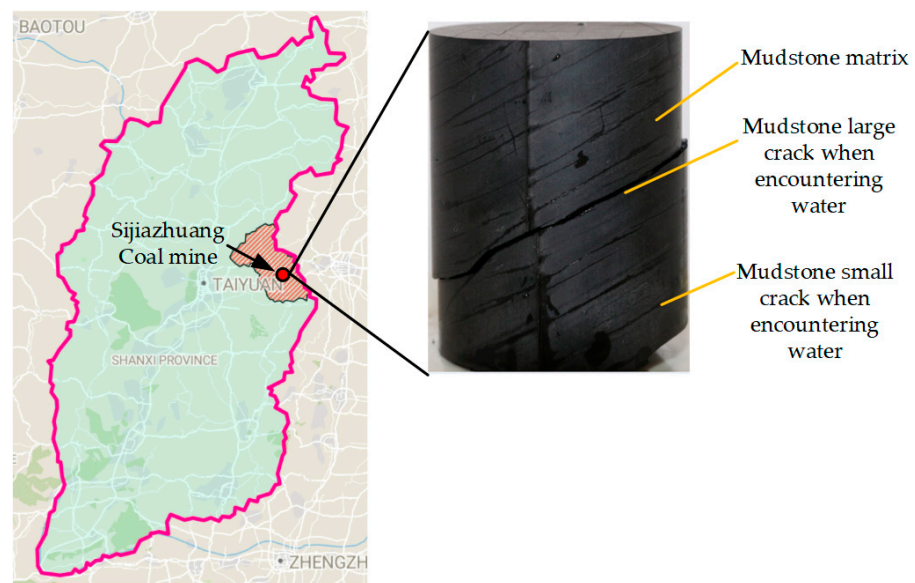


Figure 1. Location of the Sijiazhuang mine and a water decomposition diagram of mudstone.

The mineral composition of dry mudstone was analyzed through the mineral composition of the whole rock, and the distribution of the mineral composition was studied, providing a basis for the study of water seepage channels. Subsequently, a triaxial test was conducted to investigate the failure law of mudstone disintegration, determine the peak strength and residual strength under different water contents and confining pressures, and evaluate the applicability of the M–C criterion and the H–B criterion.

2.1. Composition Analysis of Mudstone

QEMSCAN model FEG Quanta 450 was employed to scan the mudstone composition at each measured location, following a process of sample polishing, extraction vacuuming, point scanning, and composition comparisons.

As illustrated in Figure 2, the mineral composition of the sampled mudstone was 73.54% kaolinite (shown in red), 11.87% pyrite (shown in yellow), and 6.31% quartz (shown in pink), and the remainder was composed of pores and other minerals. As reported in the literature [19], this type of mudstone is highly susceptible to disintegration.

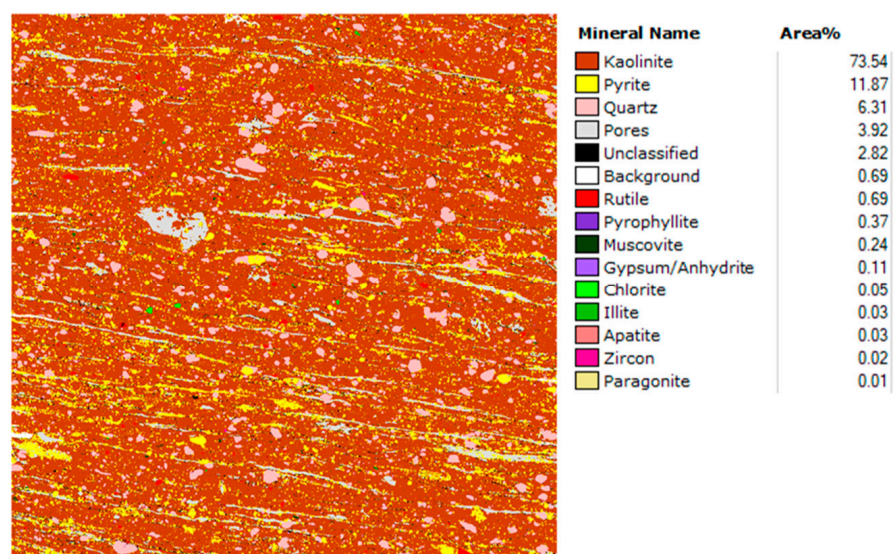


Figure 2. The mudstone mineral composition map.

The pores were extracted using the binarization method, as depicted in the dark black area in Figure 3. Two types of pore structures were observed: approximately circular solitary pores with a random distribution and inclined flat pores. In conjunction with Figure 2, it was found that pyrite was associated with such pores, which was likely due to the particle structure of pyrite and kaolinite. The particle size of pyrite is 6–10 μm , and it is cuboid in shape. The particle size of kaolinite is 2.35 μm , and it is dense and stratified. When mudstone is exposed to water, water molecules first enter the pores and then react with the kaolinite. This causes the kaolinite to expand and generate secondary cracks. Subsequently, the cracks are interconnected, leading to macro-disintegration [27].

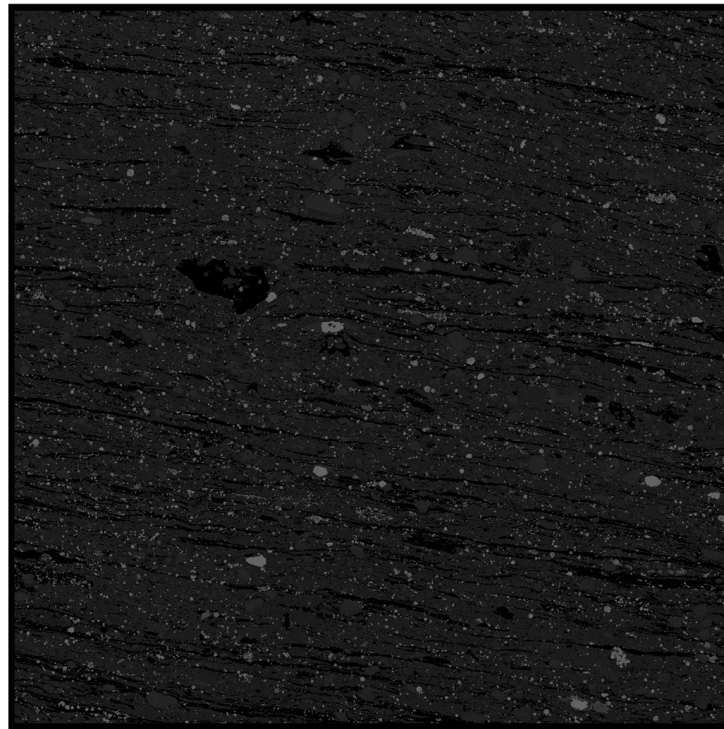


Figure 3. SEM diagram of mudstone.

2.2. Triaxial Test of Mudstone

2.2.1. Mudstone Sample Preparation and Experimental Scheme Setting

To minimize disruption during core-taking, an emery line-cutting machine was employed in the preparation process, and it did not come into contact with water. The core had a diameter of 25 mm and a height of 50 mm.

Based on the immersion test, five samples with water contents of 0%, 0.19%, 1.06%, 1.31%, and 1.40% were formulated. The in situ measured maximum ground stress and minimum principal stress of the coring position were 14.20 MPa and 7.27 MPa, respectively, resulting in four confining pressures of 0, 0.5 MPa, 7 MPa, and 14 MPa. To reduce the dispersion, three to five cores were tested for each group of confining pressures under each water content. Core number 7-3-4 indicated a confining pressure of 7 MPa and a moisture content of 1.06%, and a fourth core was tested. In the triaxial test, as shown in Figure 4, the TAW-3000 electro-hydraulic servo rock triaxial testing machine first loaded the confining pressure to the set value (0.5, 7, and 14 MPa), and then it loaded the axial pressure until the sample was damaged. The loading method used was displacement loading, and the loading rate was 1.2 mm/min.



Figure 4. TAW-3000 electro-hydraulic servo rock triaxial testing machine.

2.2.2. Analysis of the Strength Characteristics of the Mudstone

Figure 5 shows the strength curve of the mudstone under different confining pressures and water contents.

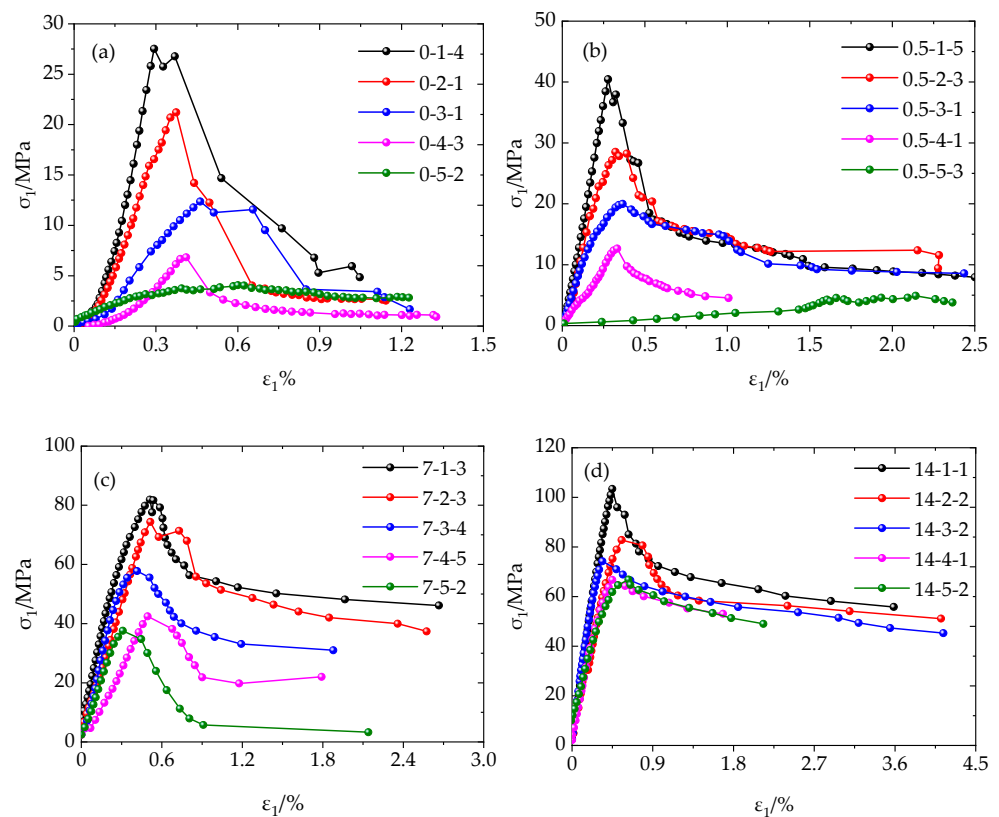


Figure 5. Stress–strain curves of the mudstone under different confining pressures and water contents: (a) confining pressure of 0 MPa; (b) confining pressure of 0.5 MPa; (c) confining pressure of 7 MPa; and (d) confining pressure of 14 MPa.

It can be observed from Figure 5 that the peak strength of the mudstone under various confining pressures decreased with the increase in the water content, particularly in the uniaxial state, in which the strength decreased more rapidly and there was almost no residual strength after the water exposure. With the increase in confining pressure, the downward trend slowed down, and the confining pressure and water content had opposite effects on the mudstone's strength. With the increase in the water content, the compaction section increased, the elastic section decreased, and the yield section increased, resulting in a larger peak strain. This was due to the fact that water entered the interior of the mudstone, causing the development of pores and fractures. It was also due to the increase in the compaction section. At the same time, due to the differences in the composition of the mudstone, the clay components first entered the yield stage when encountering the water. With the increase in axial load, components such as quartz, with their greater strength, slowly entered the yield stage. When the water content was higher, more clay components entered the yield stage, and the longer the yield section, the lower the bearing capacity. At a high water content (1.31%), mudstone undergoes a transition from brittle to plastic, with an increase in peak strain, a decrease in peak strength, and a gradual decrease in post-peak strength. Under the influence of a high confining pressure (14 MPa), mudstone also exhibits plastic deformation characteristics. It can be seen that both the water-bearing state and the stress state affect the mechanical properties of mudstone, and both have the same effect on the failure behavior of mudstone. The residual strength of mudstone with different water contents showed a significant difference under a medium confining pressure (7 MPa), while the residual strength of mudstone with different water contents under a high confining pressure (14 MPa) had little variation, indicating that the residual strength of mudstone under a medium confining pressure is greatly affected by the moisture content, while the stress under a high confining pressure has a major influence on the residual strength. A low confining pressure (0.5 MPa) had a significant impact on the peak strength of dry and low-water-content mudstone, but it had little effect on the peak strength of high-water-content mudstone. The strength of a mine support is approximately 0.1–0.7 MP, indicating that the support has an effect on the intact mudstone, with low water damage. When there are more cracks in the rock, simply increasing the support has little effect on strength improvement. The elastic modulus of mudstone with different water contents exhibited marked differences under low and medium confining pressures, while the elastic modulus of mudstone with high confining pressures remained unchanged, indicating that the water content under low and medium confining pressures had a major influence on the deformation of mudstone while the stress under high confining pressures had a major influence on or restricted the deformation. The decreased rate of the elastic modulus in a uniaxial state was 7.73 GPa/%, and the decreased rates under confining pressures of 0.5 MPa, 7 MPa, and 14 MPa were 9.93 GPa/%, 2.79 GPa/%, and 2.38 GPa/%, respectively. This indicated that the increase in the water content increased the deformation ability of the rock, but the confining pressure could effectively slow down the deformation of the rock. The two had opposite effects on the improvement of the rock's strength. Under dry conditions, the uniaxial elastic modulus of the mudstone was 13.0 GPa and the elastic modulus under a 14 MPa confining pressure was 23.9 GPa, which was an increase of 83.8%. The uniaxial elastic modulus of the mudstone with a water content of 1.40% was 1.27 GPa and the elastic modulus under a 14 MPa confining pressure was 13.55 GPa, which was an increase of 966.9%. This indicated that the increase in the confining pressure could effectively control the deformation of the rock.

In order to investigate the weakening law of peak strength, the relationship between water content and peak strength was plotted, as illustrated in Figure 6.

As can be observed in Figure 6, the peak intensity followed a linear reduction law overall, particularly in the uniaxial state. For this type of disintegrated mudstone, two significant strength reductions were observed when the water content was 0.19% and the saturated water content was 1.40%, indicating that the bearing capacity of the mudstone was significantly reduced at the initial stage of water contact and when the saturated failure

occurred. Consequently, it was advisable to avoid water contact and long-term exposure to water on the site. In a dry state, the peak strength at 7 MPa was 82.2 MPa and the peak strength at 14 MPa was 104.7 MPa, a difference of 27%. When the water content was 1.06%, the peak strength at 7 MPa was 57.77 MPa and the peak strength at 14 MPa was 75.94 MPa, a difference of 31.4%. When the water content was 1.40%, the peak strength at 7 MPa was 38.36 MPa and the peak strength at 14 MPa was 66.86 MPa, a difference of 74%. This indicated that the increase in the confining pressure on the peak strength of the fractured rock mass was more obvious.

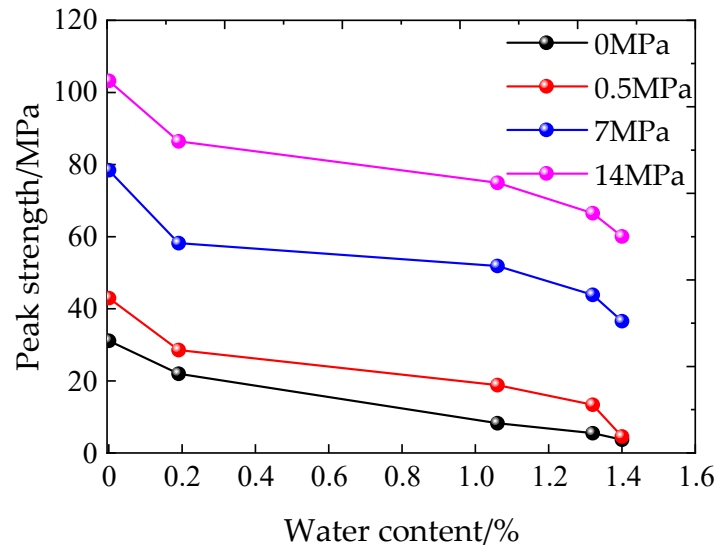


Figure 6. Relationship between different water contents and peak strength.

In order to compare the weakening law of residual strength, the relationship between water content and residual strength was drawn, as shown in Figure 7.

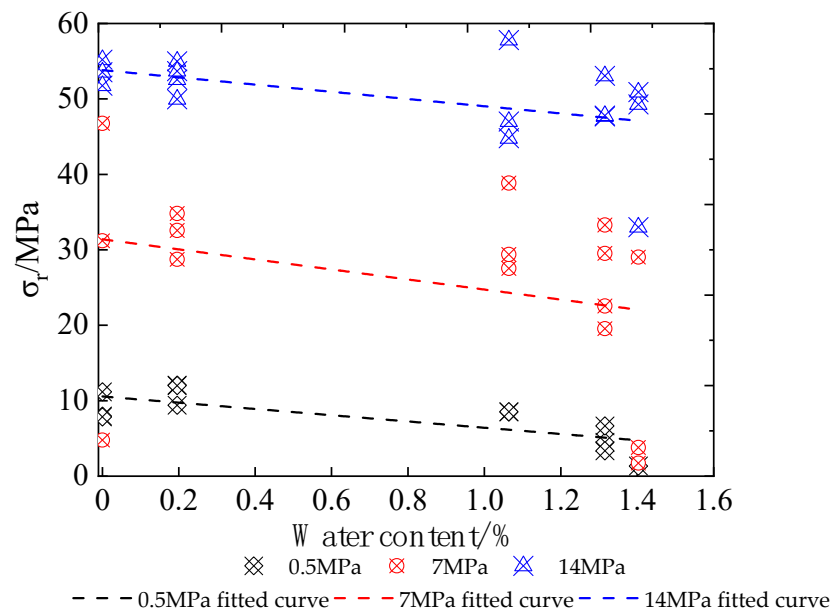


Figure 7. Relationship between different water contents and residual strengths.

As can be observed in Figure 7, except for the confining pressure of 7 MPa, the residual strengths of the different water contents under the other two confining pressures had little variation and the slopes were similar, with values of 4.15 and 4.78, respectively. It was

hypothesized that after the rock failure and loss of cohesion, the residual strength was mainly dependent on the residual friction angle. When the residual strength was similar, it suggested that the moisture content had little effect on the residual friction angle.

The linear fitting results of the relationship between peak strength, residual strength, and water content are shown in Table 1. This relationship is calculated as follows:

$$y = a + bw, \tag{1}$$

where w represents the moisture content. When it is dry, the strength is a , and b is the slope of decreasing intensity.

Table 1. Peak and residual strength water absorption fitting coefficients.

Confining Pressure	Peak Strength		Residual Strength	
	a	b	a	b
0.5	38.62	−21.37	10.56	−4.15
7	71.62	−22.45	31.39	−6.65
14	98.12	−25.05	53.81	−4.78

As can be seen in Table 1, both the peak strength and residual strength decreased linearly with the increase in the water content. The steeper the slope, the faster the rate of the decline. The rate of the decline of the peak intensity was much higher than that of the residual intensity, indicating that the water had a greater impact on peak intensity.

To compare the influence of confining pressure on residual strength and peak strength, Figure 8 was drawn.

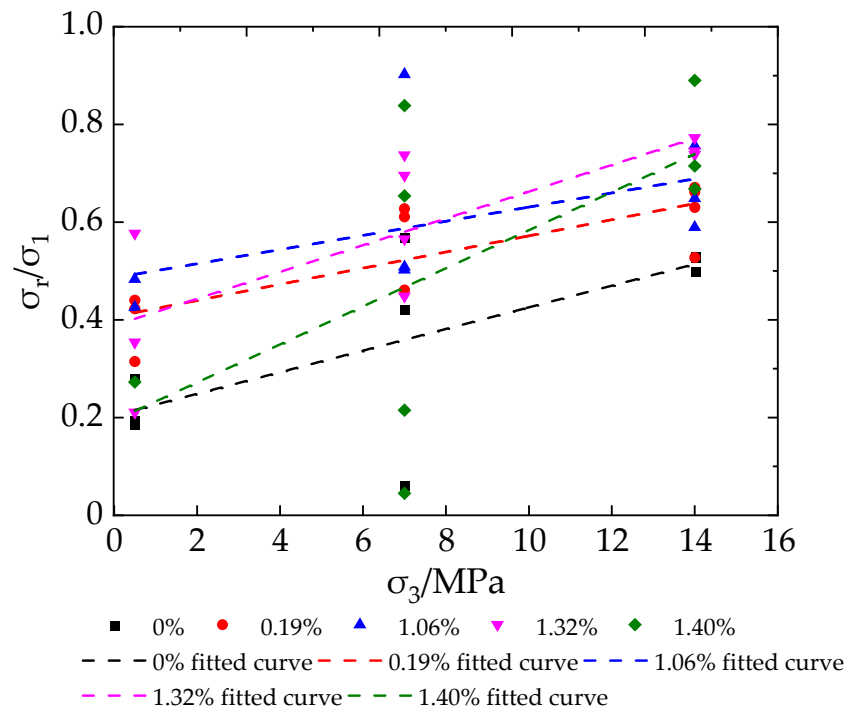


Figure 8. Residual strength vs. peak strength ratio.

As can be observed in Figure 8, the ratio of residual strength to peak strength increased with the increase in confining pressure, indicating that the confining pressure significantly increased the residual strength, thus facilitating the re-compaction of the cracks generated by the failure and the realization of the residual load through the friction effect. Under a confining pressure of 0.5 MPa, the ratio of the two was 0.2 to 0.5, and under a confining pressure of 14 MPa, the ratio of the two was 0.4 to 0.9, indicating that the residual bearing capacity of the mudstone was higher under the action of the high confining pressures in the deeper areas. Under the same confining pressure, the residual strength of the mudstone with a high water content increased more. This was due to the fact that the mudstone with a high water content had initial damage, which made it prone to failure under loading, and the peak strength was low. Confining pressure can help to re-compact the fractures generated by the failure to reach a relatively high residual strength. Previous studies [14,15] have also shown that the internal friction angles before and after rock failure change little. It was assumed that after the rock failure and loss of cohesion, the residual strength mainly depended on the residual friction angle. When the ratio of residual strength to peak strength increased with the increase in the water content, it suggested that the decrease in the residual friction angle was less than that of the cohesion.

3. Study on the Applicability of the M–C Criterion and H–B Criterion

3.1. Introduction to Rock Failure Criteria

3.1.1. M–C Criterion

When the combination of the shear stress τ and the normal stress σ_n slip plane gradually approach the boundary of the strength envelope, the rock will rupture. The two parameters, shear stress and normal stress, are formed by the axial projection of the fracture point and the stress circle, and the linear relationship between them is referred to as the Mohr–Coulomb criterion.

The M–C criterion mainly includes two variables, the cohesion c and the internal friction angle φ :

$$\tau = c + \sigma_n \tan \varphi \quad (2)$$

According to the conversion of three-way principal stress, the shear stress τ and normal stress σ_n in any plane can be expressed as follows:

$$\sigma_n = \frac{1}{2}(\sigma_1 + \sigma_3) + \frac{1}{2}(\sigma_1 - \sigma_3) \cos(2\beta) \text{ and} \quad (3)$$

$$\tau = \frac{1}{2}(\sigma_1 - \sigma_3) \sin(2\beta), \quad (4)$$

where σ_1 and σ_3 are the maximum and minimum principal stresses, and β is the angle between the direction of the maximum principal stress and the shear plane.

According to Formulas (1)–(3), the following equation can be obtained:

$$\sigma_1 = \frac{2c + \sigma_3 \{ \sin(2\beta) + \tan \varphi [1 - \cos(2\beta)] \}}{\sin(2\beta) - \tan \varphi [1 + \cos(2\beta)]} \quad (5)$$

Based on the contact position of the rupture, we can obtain:

$$\beta = \frac{\pi}{4} + \frac{\varphi}{2} \quad (6)$$

By substituting Formula (5) into Formula (4), we can obtain:

$$\sigma_1 = 2c \cdot \frac{\cos \varphi}{1 - \sin \varphi} + \frac{1 + \sin \varphi}{1 - \sin \varphi} \sigma_3 \quad (7)$$

The relationship between confining pressure and peak strength and residual strength was ascertained through a triaxial test. Fitting the results enabled the determination of the cohesion c and the internal friction angle φ .

3.1.2. H–B Criterion

The H–B criterion was initially proposed in 1980. By summarizing and analyzing a substantial amount of triaxial test data and results, it can depict the nonlinear relationship between the ultimate principal stress inside a rock, as illustrated by the following equation:

$$\sigma_1 = \sigma_3 + \sigma_c \left(m_i \frac{\sigma_3}{\sigma_c} + 1 \right)^{0.5} \quad (8)$$

where σ_1 and σ_3 are the maximum and minimum principal stresses of the rock mass failure, σ_c is the uniaxial compressive strength of intact or dry rock, and m_i is a parameter of the rock mass, which depends on the properties of the rock mass and represents the degree of rock fragmentation and disturbance. For a rock mass with a strong disturbance, $m_i = 0.001$ is used; for a hard and intact rock mass, $m_i = 25$ is recommended as the maximum value.

The formula was then updated to take into account the effects of geological conditions and blasting, as follows:

$$\sigma_1 = \sigma_3 + \sigma_c \left(m_b \frac{\sigma_3}{\sigma_c} + s \right)^a \quad (9)$$

In Formula (9), m_b , s , and a are rock mass parameters that depend on the rock mass properties. For a rock mass with a weak surface development and disturbance, $m_b = 0.001$ is taken, and for an intact rock mass without a disturbance, $m_b = 25$ is taken. For a completely broken rock mass, $s = 0$ is selected, and for an intact rock mass, $s = 1$ is selected, while a is generally selected to be 0.5.

$$m_b = m_i \exp \left(\frac{GSI - 100}{28 - 14D} \right), \quad (10)$$

$$s = \exp \left(\frac{GSI - 100}{9 - 3D} \right), \text{ and} \quad (11)$$

$$a = \frac{1}{2} + \frac{1}{6} \left(e^{-GSI/15} - e^{-20/3} \right), \quad (12)$$

where GSI is the geological strength index and D is the factor affected by blasting and other vibrations. The specific values are listed in the literature [6,7].

3.1.3. The Mutual Transformation of the M–C Criterion and the H–B Criterion

Given the widespread use of the M–C criterion, which does not account for the influence of geological parameters, such as joints and fractures on rock mass, Hoek derived the conversion relationship between the two through the fitting expression of the strength envelope, thereby indirectly calculating the internal friction angle and cohesion of the H–B criterion, which takes into account the influence of geology.

Several scholars [28,29] have compared the parameters of the H–B criterion and the M–C criterion and concluded that the H–B criterion's m_b is equivalent to the internal friction angle φ of the M–C criterion, and s is equivalent to the cohesion c .

3.2. Suitability Analysis of Peak Strength

For the M–C criterion, according to Formula (6), the angle of internal friction and the cohesion can be calculated through the slope and intercept in the coordinate system.

For the H–B criterion, m_b and s are calculated using Formula (8) and nonlinear fitting. To reduce overfitting and provide specific physical meaning to these two parameters, s was calculated first, and then m_b was fitted through nonlinear fitting. When a rock sample is

intact, $s = 1$. As the water content increases and the mudstone develops fissures, s , which represents the degree of fissure development, should be reduced.

According to Formula (8), when the confining pressure is 0, the uniaxial compressive strength is calculated as follows:

$$\sigma_1 = \sigma_c \sqrt{s}. \tag{13}$$

According to the strength of mudstone with different water contents under a uniaxial condition, s can be inversely calculated. See Table 2 for details.

Table 2. Peak strength fitting coefficient of the yield criterion.

Moisture Content	c	φ	M-C Criterion Correlation Coefficient R	m_b	s	H-B Criterion Correlation Coefficient R
0	8.40	41.57	0.91	21.25	1.00	0.50
0.19	5.91	39.04	0.92	12.26	0.50	0.73
1.06	3.41	39.64	0.94	8.92	0.07	0.95
1.32	2.37	38.32	0.92	6.37	0.03	0.93
1.40	0.94	37.29	0.82	4.10	0.01	0.82

Figure 9 shows the fitting curve of the mudstone peak strength criterion under different water contents, and the fitting parameters are shown in Table 2.

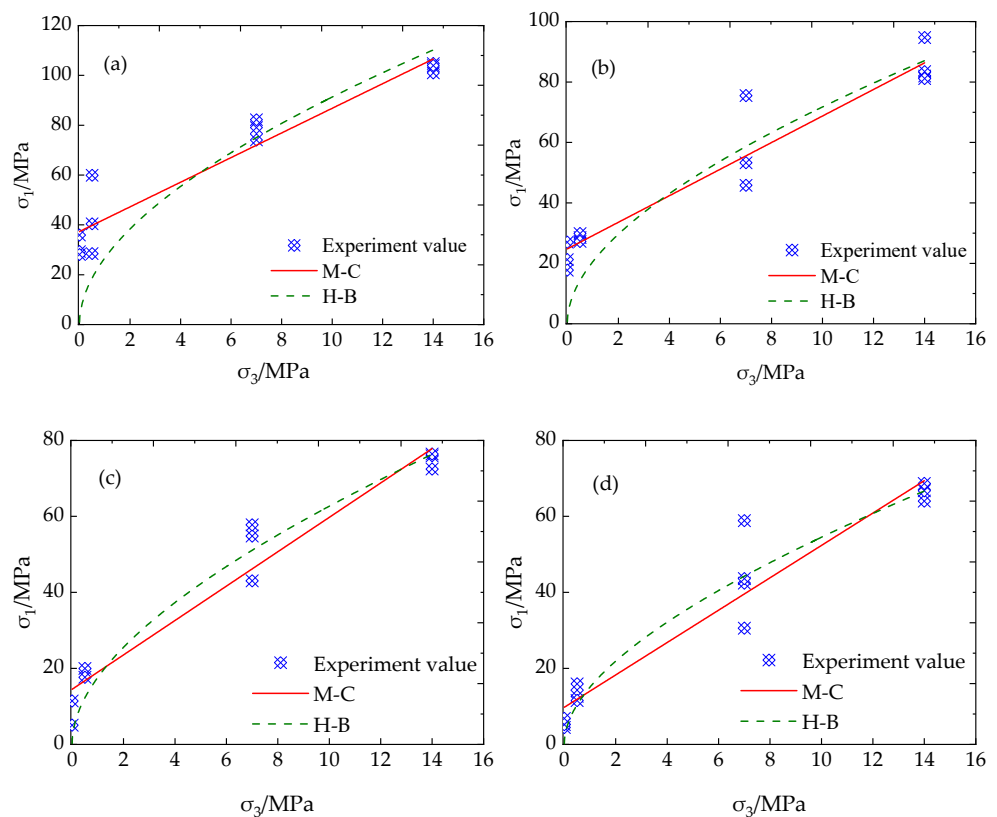


Figure 9. Cont.

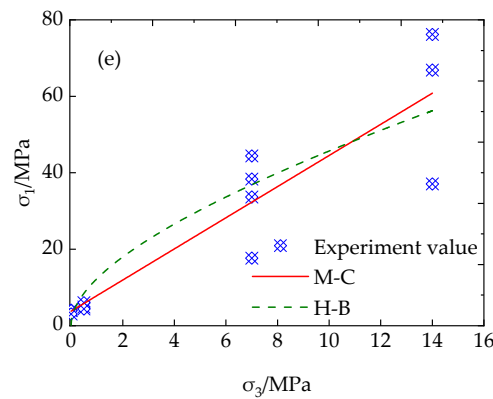


Figure 9. Fitting curves of the peak strengths of the mudstone with different water contents: (a) moisture content: 0%; (b) moisture content: 0.19%; (c) moisture content: 1.06%; (d) moisture content: 1.32%; and (e) moisture content: 1.40%.

As can be observed in Figure 9, when the moisture content is below 0.19%, the correlation coefficient of the M–C criterion is higher, indicating that it is closer to the experimental value. With the increase in the water content, the correlation coefficient of the H–B criterion is higher, indicating that the initial damage and macroscopic cracks are produced when the disintegrated mudstone is exposed to water, which is more in line with the nonlinear change law. With the increase in the water content, all the parameters decreased, but the internal friction angle decreased only slightly.

In order to compare the degree of reduction for the four variables, the case of zero moisture content was taken as the maximum value and the other indicators were divided by the maximum value for the conversion. The results are presented in Figure 10.

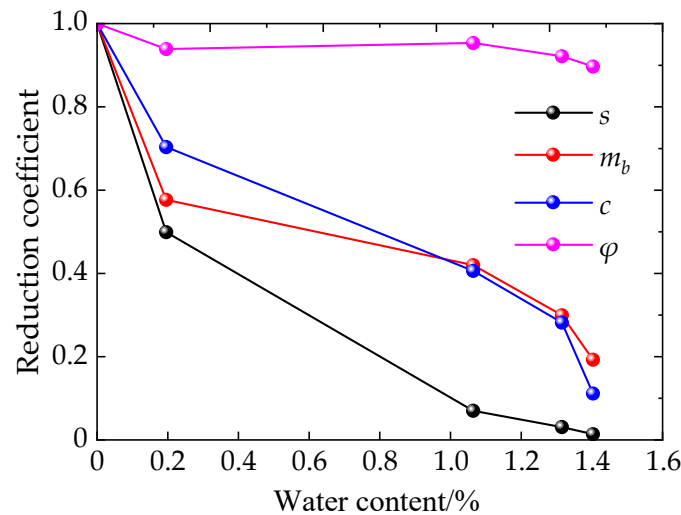


Figure 10. Plot of the reduction coefficient between the water content and the peak constitutive parameters.

As can be observed in Figure 10, the cohesion c decreased rapidly with the increase in the water content, which was in accordance with the reduction law of m_b . The internal friction angle changed only slightly, from 41.57° to 37.29° , indicating that the cohesive force of the mudstone was mainly reduced when it encountered water.

3.3. Suitability Analysis of the Residual Strength

Based on the aforementioned considerations, the parameters for residual strength were fitted. For the H–B criterion, s was assumed to be zero due to the damage that occurred in the rock mass.

As can be observed in Table 3 and Figure 11, the M–C criterion was more consistent with the change relationship between the partial residual strength and the confining pressure in terms of the correlation coefficient; however, two anomalies are present: (1) With the increase in the water content, the residual cohesion should have gradually decreased, while in the M–C criterion, the cohesion values of 1.06% and 1.32% for the water content were greater than those of the dry condition. (2) When the water content was 1.40%, the cohesion was negative, and the internal friction angle became larger. Overall, the effect of overfitting was evident.

Table 3. Residual strength fitting coefficient of the yield criterion.

Moisture Content	c	φ	M–C Criterion Correlation Coefficient R	m_b	s	H–B Criterion Correlation Coefficient R
0	1.75	32.35	0.73	3.02	0	0.74
0.19	2.82	30.67	0.99	3.36	0	0.97
1.06	2.50	30.18	0.90	2.94	0	0.92
1.32	0.82	32.72	0.95	2.40	0	0.92
1.40	−1.54	33.28	0.62	1.19	0	0.56

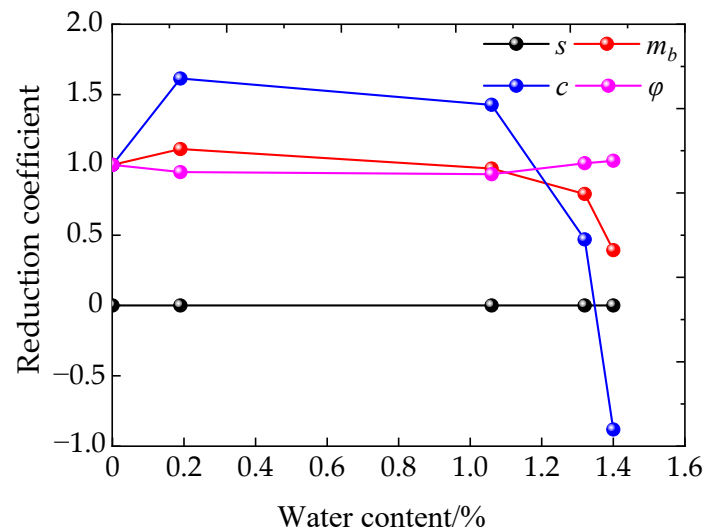


Figure 11. Plot of the reduction coefficient between the moisture content and the residual constitutive parameters.

The correlation coefficient R in Table 3 is a measure describing the degree of strong correlation between two variables, and the absolute value of R can be between 0 and 1. Generally speaking, the closer R is to 1, the stronger the correlation between X and Y . Conversely, the closer R is to 0, the weaker the correlation between X and Y . The value of R can be calculated as follows:

$$R = \frac{\sum_{i=1}^n (X_i - \bar{X})(Y_i - \bar{Y})}{\sqrt{\sum_{i=1}^n (X_i - \bar{X})^2} \sqrt{\sum_{i=1}^n (Y_i - \bar{Y})^2}}. \quad (14)$$

When the water content reached 1.40%, the fitting degree of the two criteria was not satisfactory. This was due to the fact that the dominant fracture surface was generated after the water encounter, and the damage occurred along the dominant fracture surface. Since the medium was not isotropic, it could not be adapted to the aforementioned criteria. Consequently, the H–B criterion is recommended for the residual strength.

4. Discussion

In order to illustrate the influence of confining pressure and water content on the failure forms of mudstone, nine failure forms were selected under the conditions of a low confining pressure of 0.5 MPa, a middle confining pressure of 7 MPa, and a high confining pressure of 14 MPa, with corresponding water contents of zero, 1.06%, and 1.40%, respectively.

As can be seen in Figures 12–14, the increase in the water content led to an intensification of mudstone damage, resulting in an increase in fragments. At the low confining pressure of 0.5 MPa, the penetrating failure surface of the dry mudstone was approximately vertical, which was close to uniaxial failure. Water-bearing mudstone has a variety of fractures, with many fragments that are difficult to form after failure. Under the confining pressure of 7 MPa, the dry mudstone had a single inclined shear failure surface, while the water-bearing mudstone had a variety of fractures, accompanied by weak shear failure. Under the high confining pressure of 14 MPa, the dry mudstone produced a single shear failure surface, while the water-bearing mudstone produced a single fracture, primarily a single shear failure surface, with other shear failures mixed around the main failure surface.

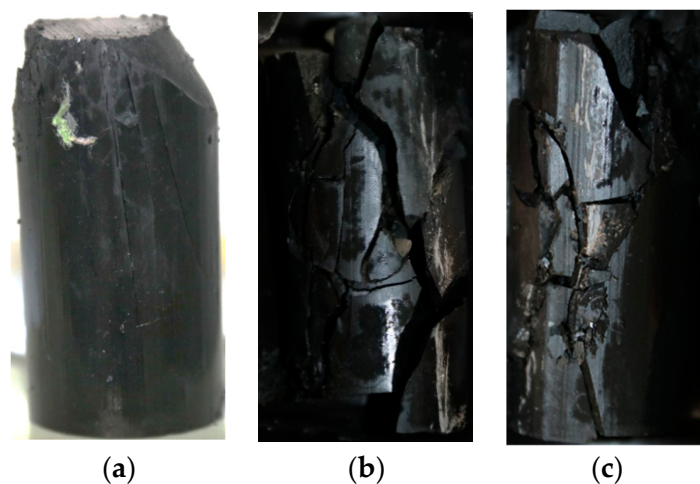


Figure 12. Damage diagram under a 0.5 MPa confining pressure: (a) moisture content: 0%; (b) moisture content: 1.06%; and (c) moisture content: 1.40%.

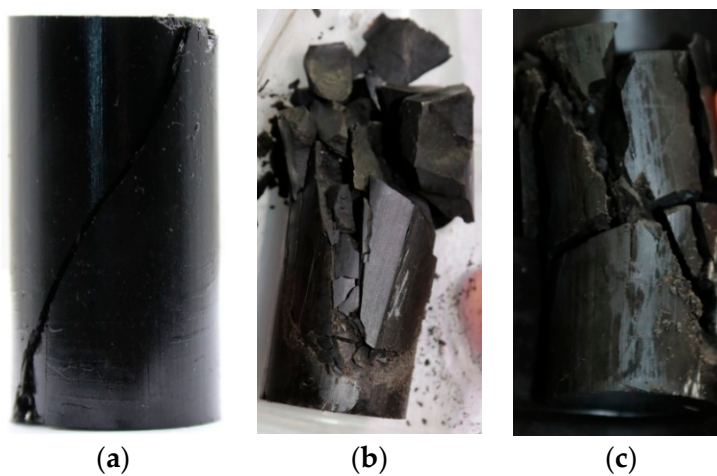


Figure 13. Damage diagram under a 7 MPa confining pressure: (a) moisture content: 0%; (b) moisture content: 1.06%; and (c) moisture content: 1.40%.

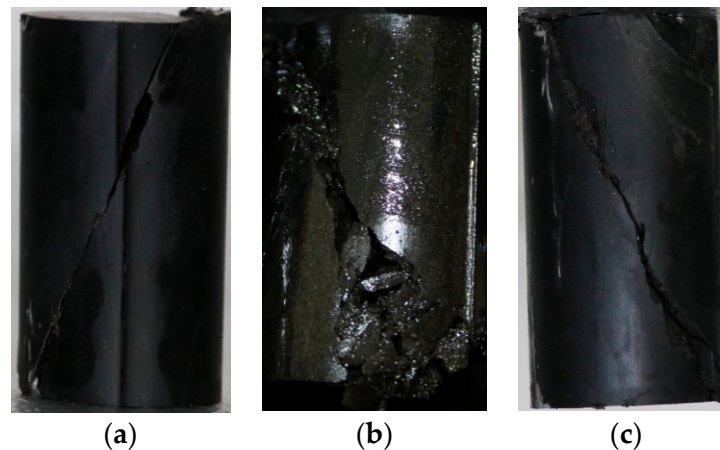


Figure 14. Damage diagram under a 14 MPa confining pressure: (a) moisture content: 0%; (b) moisture content: 1.06%; and (c) moisture content: 1.40%.

These results suggested that the fractures caused by the initial damage to the mudstone from the water were predominantly failure forms under low and middle confining pressures, and they exhibited varied failure forms. Under a high confining pressure, the fracture surface was a single inclined plane shear failure, and the water guided the fissure generated by the initial damage to the mudstone. Ultimately, the fracture along this fissure was consistent with shear failure, resulting in a single failure form.

5. Conclusions

(1) The peak strength and residual strength of mudstone follow a linear reduction law with increasing water content, with the peak strength decreasing at a faster rate than the residual strength.

(2) The decrease in strength caused by the increase in water content is mainly attributed to the decrease in cohesion, with the peak strength cohesion decreasing from 8.40 MPa to 0.94 MPa and the residual strength cohesion decreasing from 1.75 MPa to 0.82 MPa. The internal friction angle of the peak strength decreased from 41.57° to 37.29° while the post-peak internal friction angle increased from 32.35° to 33.28° .

(3) For dry mudstone with a low water content, the peak strength conforms to the Mohr–Coulomb criterion, while for mudstone with a high water content, the peak strength conforms to the Hoek–Brown criterion. The residual strength conforms to the Hoek–Brown criterion. However, when the moisture content increases and more cracks occur, the medium is no longer isotropic, rendering the two failure criteria inapplicable.

(4) The moisture content under a medium confining pressure has a significant impact on the residual strength of mudstone, while the stress under a high confining pressure has a significant influence on the residual strength. Moreover, compared to peak strength, the confining pressure increases the residual strength more significantly.

(5) Under low and medium confining pressures, the fractures caused by initial water damage to mudstone are the primary contributors to the failure forms, which are varied. However, under a high confining pressure, water guides the fissure generated by the initial damage to the mudstone, resulting in a single failure form that conforms to shear failure.

Author Contributions: Conceptualization, Y.L.; methodology, D.W.; validation, Y.L.; investigation, Y.L. and D.W.; resources, Y.L.; data curation, Y.L.; writing—original draft preparation, Y.L.; writing—review and editing, Y.L. and D.W.; visualization, D.W. All authors have read and agreed to the published version of the manuscript.

Funding: This article was funded by the National Natural Science Foundation of China Youth Foundation Project (grant number 52104091) and the CCTEG Coal Mining Research Institute Science and Technology Innovation Fund (grant number KCYJY-2022-MS-01).

Institutional Review Board Statement: Not applicable.

Informed Consent Statement: Not applicable.

Data Availability Statement: Contact corresponding authors for data.

Conflicts of Interest: The authors declare no conflict of interest.

References

1. Cai, M.F. *Rock Mechanics and Engineering Science*; China Science Publishing & Media Ltd. Press: Beijing, China, 2001.
2. Hoek, E.; Brown, E.T. *Underground Excavation in Rock*; Institution of Mining and Metallurgy: London, UK, 1980.
3. Rafiei Renani, H.; Cai, M. Forty-Year Review of the Hoek–Brown Failure Criterion for Jointed Rock Masses. *Rock Mech. Rock Eng.* **2022**, *55*, 439–461. [[CrossRef](#)]
4. Singh, M.; Raj, A.; Singh, B. Modified Mohr–Coulomb criterion for non-linear triaxial and polyaxial strength of intact rocks. *Int. J. Rock Mech. Min. Sci.* **2011**, *48*, 546–555. [[CrossRef](#)]
5. Singh, M.; Singh, B. Modified Mohr–Coulomb criterion for non-linear triaxial and polyaxial strength of jointed rocks. *Int. J. Rock Mech. Min. Sci.* **2012**, *51*, 43–52. [[CrossRef](#)]
6. Hoek, E.; Carranza-Torres, C.; Corkum, B. Hoek–Brown failure criterion—2002 edition. In Proceedings of the Fifth North American Rock Mechanics Symposium (NARMS-TAC), Toronto, ON, Canada, 7–10 July 2002; University of Toronto Press: Toronto, ON, Canada, 2002; pp. 267–273.
7. Eberhardt, E. The Hoek–Brown Failure Criterion. *Rock Mech. Rock Eng.* **2012**, *45*, 981–988. [[CrossRef](#)]
8. Mehranpour, M.H.; Kulatilake, P.H.S.W.; Ma, X.; He, M. Development of new three-dimensional rock mass strength criteria. *Rock Mech. Rock Eng.* **2018**, *51*, 3537–3561. [[CrossRef](#)]
9. Rafiai, H. New empirical polyaxial criterion for rock strength. *Int. J. Rock Mech. Min. Sci.* **2011**, *48*, 922–931. [[CrossRef](#)]
10. Fathipour-Azar, H. Polyaxial rock failure criteria: Insights from explainable and interpretable data-driven models. *Rock Mech. Rock Eng.* **2022**, *55*, 2071–2089. [[CrossRef](#)]
11. He, M.; Zhang, Z.; Zhu, J.; Li, N. Correlation between the constant m_i of hoek–Brown criterion and porosity of intact rock. *Rock Mech. Rock Eng.* **2022**, *55*, 1–14. [[CrossRef](#)]
12. Wu, L.Y.; Wang, Z.; Ma, D.; Zhang, J.W.; Wu, G.; Wen, S.; Zha, M.; Wu, L. A Continuous Damage Statistical Constitutive Model for Sandstone and Mudstone Based on Triaxial Compression Tests. *Rock Mech. Rock Eng.* **2022**, *55*, 4963–4978. [[CrossRef](#)]
13. Sun, C.; Hui, X.-M.; Zhang, Q. Study on post peak strain softening behavior of mudstone and the interaction between surrounding rock and supporting structure interaction. *J. China Univ. Min. Technol.* **2016**, *45*, 254–260.
14. Wang, L.-G.; Zhang, H.-J.; Zhang, C.-H.; Pan, J.W.; Zhao, N. Experimental investigation on the effects of confining pressure and moisture content on post-peak mechanical behavior of anjialing mudstone. *Exp. Mech.* **2016**, *31*, 683–693.
15. Cai, M.; Kaiser, P.; Tasaka, Y.; Minami, M. Determination of residual strength parameters of jointed rock masses using the GSI system. *Int. J. Rock Mech. Min. Sci.* **2007**, *44*, 247–265. [[CrossRef](#)]
16. Walton, G.; Arzúa, J.; Alejano, L.R.; Diederichs, M.S. A laboratory-testing-based study on the strength, deformability, and dilatancy of carbonate rocks at low confinement. *Rock Mech. Rock Eng.* **2015**, *48*, 941–958. [[CrossRef](#)]
17. Dong, F. *Supporting Theory and Application Technology of Roadway Surrounding Rock Loose Zone*; China Coal Industry Press: Beijing, China, 2001.
18. Jing, W.; Xue, W.; Yao, Z. Variation of the internal friction angle and cohesion of the plastic softening zone rock in roadway surrounding rock. *J. China Coal Soc.* **2018**, *43*, 2203–2210.
19. Yao, Q.L.; Wang, W.N.; Li, X.H.; Tang, C.J.; Xu, Q.; Yu, L.Q. Study of mechanical properties and acoustic emission characteristics of coal measures under water-rock interaction. *J. China Univ. Min. Technol.* **2021**, *50*, 558–569.
20. Zhang, H.-Q.; He, Y.-N.; Zhou, J.-J.; Han, L.J.; Jiang, B.S.; Shao, P. Experiment study of the strength evolution laws in rock failure process. *J. Rock Mech. Eng.* **2010**, *29*, 3273–3279.
21. Xiong, D.G.; Zhao, Z.M.; Su, C.D.; Wang, G.Y. Experimental study of effect of water-saturated state on the mechanical properties of rock in coal measure strata. *J. Rock Mech. Eng.* **2011**, *30*, 998–1006.
22. Zhu, J.; Deng, J.; Chen, F.; Wang, F. Failure analysis of water-bearing rock under direct tension using acoustic emission. *Eng. Geol.* **2022**, *299*, 106541. [[CrossRef](#)]
23. Małkowski, P.; Ostrowski, Ł.; Stasica, J. Modeling of floor heave in underground roadways in dry and waterlogged conditions. *Energies* **2022**, *15*, 4340. [[CrossRef](#)]
24. Wang, K.; Feng, G.; Bai, J.; Guo, J.; Shi, X.; Cui, B.; Song, C. Dynamic behaviour and failure mechanism of coal subjected to coupled water-static-dynamic loads. *Soil Dyn. Earthq. Eng.* **2022**, *153*, 107084. [[CrossRef](#)]
25. Luo, Y.; Gong, F.; Zhu, C. Experimental investigation on stress-induced failure in D-shaped hard rock tunnel under water-bearing and true triaxial compression conditions. *Bull. Eng. Geol. Environ.* **2022**, *81*, 76. [[CrossRef](#)]
26. Xue, Y.; Ranjith, P.G.; Gao, F.; Zhang, Z.; Wang, S. Experimental investigations on effects of gas pressure on mechanical behaviors and failure characteristic of coals. *J. Rock Mech. Geotech. Eng.* **2023**, *15*, 412–428. [[CrossRef](#)]
27. Qu, Y.-X. The engineering classification and fast forecast of swelling potential energy of mud rock. *J. Hydrogeol. Eng. Geol.* **1988**, *5*, 36–39.

28. Day, J.J.; Hutchinson, D.J.; Diederichs, M.S. A critical look at geotechnical classification for rock strength estimation. In Proceedings of the 46th US Rock Mechanics/Geomechanics Symposium, Chicago, IL, USA, 24–27 June 2012; American Rock Mechanics Association: Alexandria, VA, USA, 2012.
29. Crowder, J.J.; Bawden, W.F. Review of post-peak parameters and behaviour of rock masses: Current trends and research. *Rocnews Fall* **2004**, *13*, 1–14.

Disclaimer/Publisher's Note: The statements, opinions and data contained in all publications are solely those of the individual author(s) and contributor(s) and not of MDPI and/or the editor(s). MDPI and/or the editor(s) disclaim responsibility for any injury to people or property resulting from any ideas, methods, instructions or products referred to in the content.